DOI: 10.1002/adma.200600685

Anisotropic Growth of PbSe Nanocrystals on Au–Fe_3O_4 Hybrid Nanoparticles**

By *Weili Shi*, *Yudhisthira Sahoo*, *Hao Zeng*,* *Yong Ding*, *Mark T. Swihart*,* and *Paras N. Prasad**

Two of the most important research directions in the preparation of nanocrystals are the growth of non-spherical quantum-confined structures and nanocrystal heterostructures. Non-spherical structures provide a means of understanding the effect of dimensionality and structural anisotropy on quantum-confined optoelectronic behavior and also introduce new degrees of freedom in engineering nanocrystal-based devices. Semiconductor nanorods have potential technological advantages over spherical nanocrystals in applications such as polarized light emitters[1] and photovoltaics.[2] Preparation of nanocrystal heterostructures enables new combinations of material properties, such as photonic and magnetic properties, to be achieved. This opens up new possibilities for investigating interactions between nanoscale components of different materials, and new technological applications based on combinations of material properties not attainable in homogeneous nanocrystals. Colloidal chemistry provides the basis of a modular approach for integrating different materials and, therefore, different functionalities in these nanocrystal heterostructures.

Anisotropic growth of semiconductors with the wurtzite crystal structure has been achieved using multiple surfactants, exploiting inherent differences in growth rates between different crystal directions,[3,4] which are modulated by differences in the affinity of surfactants for the different crystal faces. In other cases, a solution-liquid-solid (SLS) method that employs molten metal particles as seeds for heterogeneous nucleation and growth of semiconductor wires has been used.[5–13] For groups IV, II–VI, and III–V materials, there is a substantial body of knowledge on the growth of anisotropic nanostructures. However, understanding of anisotropic growth of IV–VI materials is less well developed. Hull et al. have prepared long, branched PbSe wires using an SLS approach,[11] and Cho et al. have prepared PbSe nanowires and nanorings via controlled oriented aggregation of PbSe particles.[14] However, these methods do not provide a route to dispersible nanorods with tunable length and aspect ratio that can be chemically processed. Yong et al. recently reported noble metal seeded growth of PbSe nanorods and branched nanostructures[15] using extremely low concentrations of metal nanoparticles. Although the effect of the metal seed particles on PbSe morphology in that study was clear, no direct evidence of PbSe rods growing from the metal seeds was presented, and no free Au seed particles could be found in the reaction products, probably because of the extremely low seed particle concentrations used. Thus, the mechanism of this effect on morphology remained somewhat unclear. For InAs and InP, mixtures of rods and wires of different lengths were synthesized by Kan et al. using Au nanoparticles as seeds,[16] followed by multiple steps of centrifugation to achieve length control.

Here, we present a technique to grow PbSe nanocrystals with different morphologies (dotlike, rodlike, and branched) on Au–Fe_3O_4 binary hybrid nanoparticles. The Au–Fe_3O_4 binary hybrid nanoparticles are 'peanut-shaped', each consisting of a smaller spherical Au nanoparticle attached to, and slightly embedded in, a larger Fe_3O_4 nanoparticle, as shown in the center of Figure 1 and also in Figure S1 in the Supporting Information. When these particles are used to seed growth of PbSe, the semiconductor nucleates only on the Au portion, initially forming ternary hybrid nanoparticles. By varying the PbSe precursor-to-seed particle ratio, the extent of growth can be controlled to yield a dot-shaped PbSe component (structure **1** in Fig. 1), a rod-shaped PbSe component (structures **2a** and **2b**), multiple rod-shaped PbSe components (structures **3a** and **4a**) or a multibranched PbSe component (structures **3b**, **4b**, and **5**). The dominant observed morphology proceeds clockwise from structure **1** to structure **5** as the precursor-to-seed ratio is increased, but multiple morphologies may co-exist in the same sample. Rod-shaped and multibranched PbSe components cleave from the Au–Fe_3O_4 binary

[*] Prof. H. Zeng
Department of Physics, University at Buffalo (SUNY)
Buffalo, NY 14260 (USA)
E-mail: haozeng@buffalo.edu
Prof. M. T. Swihart, W. Shi
Department of Chemical and Biological Engineering
University at Buffalo (SUNY)
Buffalo, NY 14260 (USA)
E-mail: swihart@eng.buffalo.edu
Prof. P. N. Prasad, Prof. Y. Sahoo
Department of Chemistry, University at Buffalo (SUNY)
Buffalo, NY 14260 (USA)
E-mail: pnprasad@buffalo.edu
Prof. M. T. Swihart, Prof. P. N. Prasad, W. Shi, Prof. Y. Sahoo
Institute for Lasers, Photonics, and Biophotonics
University at Buffalo (SUNY)
Buffalo, NY 14260 (USA)
Dr. Y. Ding
School of Materials Science and Engineering
Georgia Institute of Technology
Atlanta, GA 30332 (USA)

[**] This work was supported by a Defense University Research Initiative on Nanotechnology grant, through the Chemistry and Life Sciences Directorate of the Air Force Office of Scientific Research, and by the US National Science Foundation, through grant number DMR-0547036. Supporting Information is available online from Wiley InterScience or from the author.

ADVANCED MATERIALS

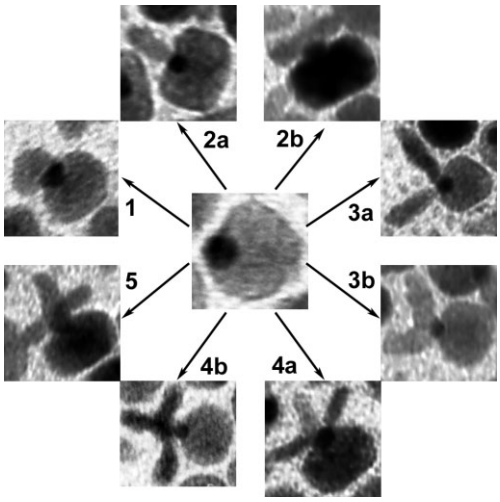

Figure 1. Transmission electron microscopy (TEM) images illustrating the different growth morphologies of PbSe on Au–Fe_3O_4.

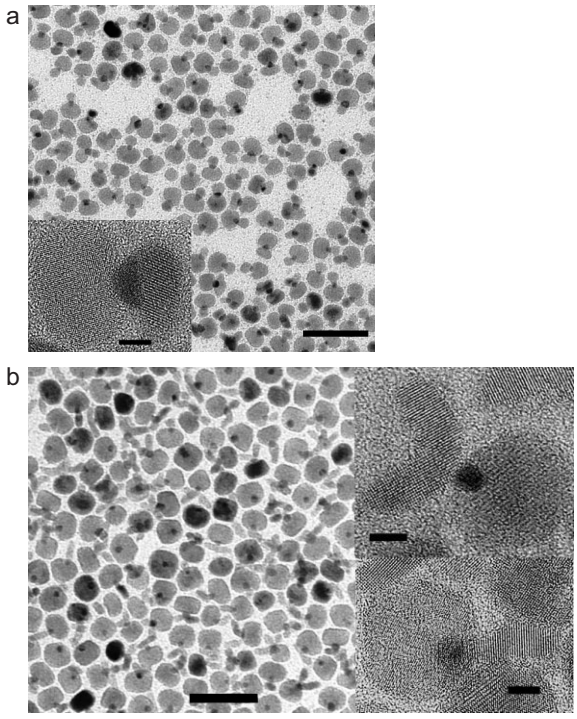

Figure 2. TEM and high-resolution TEM (HRTEM) images of PbSe nanodots (a) and nanorods (b) grown on Au–Fe_3O_4 hybrid nanoparticles. The scale bars are 50 and 4 nm for the low- and high-resolution images, respectively.

nanoparticles when their length exceeds a critical value, giving rise to freestanding PbSe nanocrystals. Length control of free PbSe nanorods is achieved by extracting products after different reaction times. Without any size selection, size distributions as narrow as ±10 % in diameter and ±15 % in length were realized. In ternary nanoparticles, Fe_3O_4 provides a magnetic 'handle' that may allow nanocrystal self-assembly and orientation to be guided by an applied magnetic field. Thus, the present study is focused both on providing an improved method for preparing freestanding, simple, and branched PbSe nanorods of controlled size and aspect ratio, based on the advantageous properties of the binary hybrid nanoparticles used here as seeds, and on preparing ternary nanoparticles with an anisotropic PbSe component.

The morphology of the PbSe nanocrystals can be controlled, as illustrated in Figure 1, by changing the seed particle-to-precursor ratio. Increasing the seed particle concentration at fixed precursor concentration resulted in ternary hybrid nanoparticles, with PbSe dots forming on the Au–Fe_3O_4 binary particles (structure **1** in Fig. 1).[17] In that case, no free PbSe nanocrystals are observed, even at long reaction times, as shown in Figure 2a. Decreasing the seed particle concentration by a factor of two (doubling the precursor-to-seed ratio) led to the growth of PbSe rods (predominantly structures **2a** and **2b** in Fig. 1). Decreasing the seed particle concentration by a factor of four resulted in branched PbSe nanocrystals (predominantly structures **3a** to **5** in Fig. 1). At long reaction times, the rods and branched nanocrystals detached from the seed particles, yielding free PbSe nanocrystals. We observed the evolution of PbSe size and morphology through transmission electron microscopy (TEM) imaging of particles sampled at different times during the course of the reaction.

For an intermediate seed concentration and an initial reaction temperature of ca. 125 °C, there was an induction period during which no PbSe nanocrystals were observed. Under these conditions, the first PbSe formation was observed about 4 min after Se injection. Between 4 and 7 min after Se injection, we observed ternary heterostructures consisting of spherical lobes of Au and Fe_3O_4 and one or more rods of PbSe, along with both free PbSe rods and binary Au–Fe_3O_4 seed particles. After 7 min, nearly all of the PbSe rods and Au–Fe_3O_4 seed particles were separated, and very few ternary structures were observed. In all the ternary heterostructrures, PbSe was anchored only to the Au domain and never grew on the Fe_3O_4. When the reaction was carried out at ca. 155 °C using smaller solvent volumes, the induction period for PbSe formation was much reduced, and similar ternary nanostructures were obtained 30 s after Se injection. Figure 2b presents TEM images of such a sample, extracted after 30 s of reaction at 155 °C. Even at this short reaction time, many rods have already cleaved from the ternary hybrid nanoparticles, and both free PbSe rods and binary Au–Fe_3O_4 particles are present.

Figure 3 shows typical TEM images of free PbSe nanocrystals prepared using Au–Fe_3O_4 seeds. Figure 3a shows the final product (ca. 9 min after Se injection) from a reaction carried out at ca. 125–135 °C; the product is a mixture of PbSe rods and seed particles, with almost no ternary structures remaining. Figure 3b–f shows PbSe rods obtained after different reaction times and under different conditions, and demonstrates the control over rod length and aspect ratio that can be achieved by varying these parameters while keeping the quantities of the seed particles and precursors fixed. The PbSe rods shown in Figure 3b–d were grown at ca. 125–135 °C and ex-

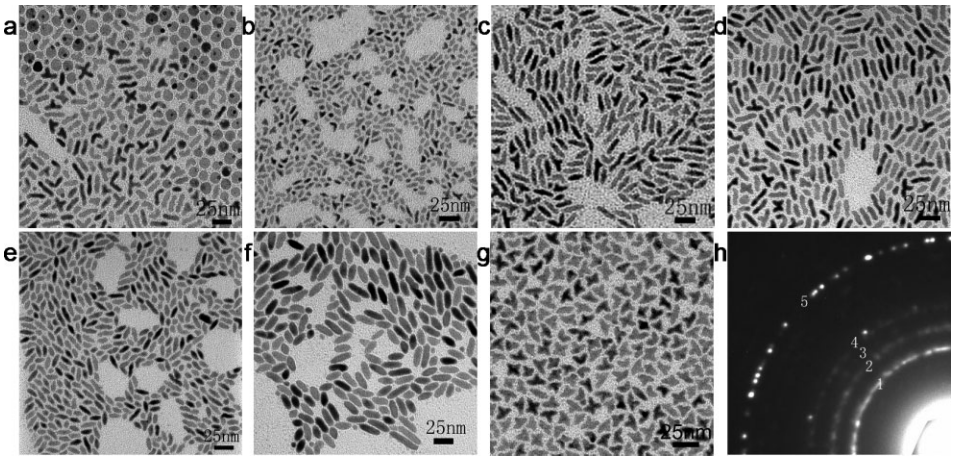

Figure 3. TEM images of and electron diffraction from PbSe nanocrystals. a–d,g) Reactions carried out at ca. 125–135 °C, e,f) reaction carried out at ca. 155 °C. a) Final products as a mixture of Au–Fe_3O_4 seeds and PbSe rods. PbSe nanorods extracted at b) 4, c) 7, d) 9 min, e) 30, and f) 90 s after selenium injection. g) TEM image of branched PbSe nanocrystals produced after 8 min of reaction at ca. 125–135 °C using 1/2 the quantity of seed particles used for the samples shown in parts (a) to (f). h) Typical electron diffraction pattern of final products like those shown in (a). Rings are indexed as follows: 1 PbSe {200}, 2 Fe_3O_4 {311}, 3 Au {111}, 4 PbSe {220}, and 5 Fe_3O_4 {440}.

tracted at 4, 7, and 9 min after Se-trioctylphosphine (Se–TOP) injection, respectively. The mean lengths and diameters, respectively, are 10 ± 1.5 and 2.5 ± 0.5 nm in Figure 3b, 19 ± 3 and 3 ± 0.5 nm in Figure 3c, and 23.5 ± 4.5 and 4.6 ± 0.5 nm in Figure 3d. The PbSe rods shown in Figure 3e and f were grown at ca. 153–157 °C and extracted 30 and 90 s after Se–TOP injection. Their mean lengths and diameters, respectively, are 16.8 ± 5.4 and 5.4 ± 0.8 nm in Figure 3e, and 22 ± 6.5 and 7 ± 1 nm in Figure 3f. In most cases, a small amount of L-, T-, and cross-shaped branched PbSe nanocrystals are also present, but simple rods dominate the population for this intermediate seed particle concentration. Here, we emphasize that although selective precipitation can be used to separate the PbSe rods from the seed particles, no size selection has been performed on the samples presented in Figure 3.

The critical factors in determining the length and diameter of the PbSe rods are reaction temperature, growth time, and precursor concentration. As can be seen by comparing Figure 3c and d with Figure 3e and f, at higher injection and growth temperature and higher precursor concentration (with fixed precursor and seed quantities and reduced amount of solvent), the resulting rods had lower aspect ratios. The length of the PbSe rods increased with growth time, apparently until the 9-octadecenoic acid (Z)-, lead salt (Pb-oleate) precursor was depleted, with a higher growth rate in the axial direction than in the radial direction. So, increasing the reaction temperature and precursor concentrations increases both the axial and radial growth rates, yet decreases the aspect ratio of the rods. The overall simple rod morphology did not change substantially over the range of concentrations and temperatures used in these experiments, provided that the ratio of precursors to seed particles remained fixed.

Figure 3g shows a typical TEM image of branched PbSe nanocrystals, produced by halving the quantity of binary nanoparticle seeds used to form the PbSe rods. About 4 % of the particles observed in this sample are simple PbSe rods, 5 % are L shaped, 66 % are T shaped, and the remaining 25 % are cross shaped. The different branches grow uniformly perpendicular to each other. The high percentage of T- and cross-shaped nanocrystals results from ternary nanoparticles like structures **4** and **5** displayed in Figure 1. Figure 3h shows a typical electron diffraction pattern of the mixed final products like those shown in Figure 3a, containing both PbSe rods and Au–Fe_3O_4 hybrid nanoparticles. It shows the expected ring patterns from PbSe, Au, and Fe_3O_4, consistent with the rock salt structure of PbSe, the face centered cubic (fcc) structure of Au, and the cubic spinel structure of Fe_3O_4. The samples shown in Figure 3 were also characterized by optical absorption spectroscopy, shown in Figure S2 in the Supporting Information. The absorption measurements suggest that the onset of absorbance lies beyond the upper limit (2000 nm) of the measurement. This is not surprising, given that the bandgap of bulk PbSe (0.28 eV) corresponds to a wavelength near 4400 nm. The absorption peaks are broad, presumably due both to the anisotropic shape of the nanocrystals, which leads to different degrees of quantum confinement in different directions, and due to the presence of a distribution of nanocrystal sizes in each sample. The expected shift of the absorption onset to higher wavelengths (lower energy) with increasing nanocrystal size due to decreased quantum confinement is thus not obvious from these measurements, but may be inferred by extrapolating the absorption peaks to longer wavelengths.

In Figure 4 high-resolution TEM (HRTEM) images of several PbSe nanocrystals are displayed. Examination of these images and many others like them shows that the (200) lattice planes are always oriented perpendicular to the growth direction, in both the simple rods and the branched structures. In the branched structures this requires that the arms be oriented perpendicular to each other as is uniformly observed in the

ADVANCED MATERIALS

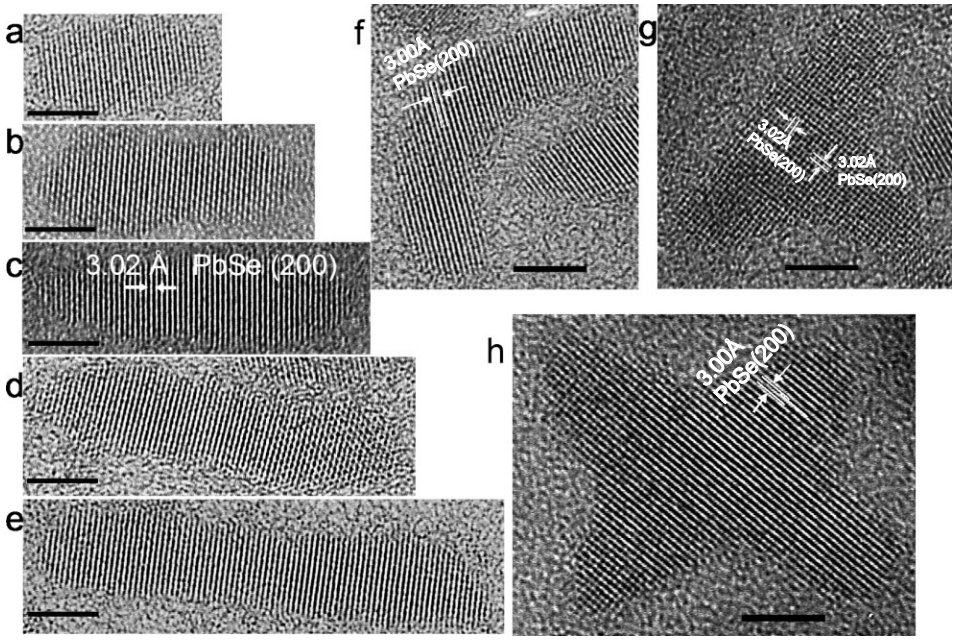

Figure 4. HRTEM images of typical PbSe nanocrystals, including rods of different lengths: a) 9.8, b) 14.6, c) 17.8, d) 20.8, and e) 25.6 nm. Typical f) L-, g) T-, and h) cross-shaped branched nanocrystals.

low-resolution TEM images, where L-, T-, and cross-shaped particles are observed, but no Y-shaped structures are present. This is consistent with recent observations of PbSe wires prepared by other methods,[11,14] in which the wire axis was always aligned with the <200> direction of the crystal lattice.

In previous reports of metal-seeded solution-phase synthesis of crystalline semiconductor nanowires[5–13] and nanorods,[16] the growth has usually been interpreted in terms of the SLS mechanism proposed by Trentler et al.[5] In the present case, the Au component of the binary particle clearly seeds PbSe growth, but it probably is not molten under the growth conditions. Even accounting for the reduction of the melting point due to finite size effects,[18] temperatures above 600 °C are required to melt 3 nm Au particles. The Au–Pb phase diagram[19] shows that lower-melting-point solutions can form, down to the $AuPb_2$–Pb eutectic temperature of 215 °C. However, no free Pb or Au–Pb compounds have been observed in any of the reaction products. Thus, it appears that the essential contribution of the seed particle is to provide a low-energy interface for heterogeneous nucleation of the PbSe crystalline phase. Initially, a PbSe dot nucleates. If sufficient precursors remain available this nucleus then grows anisotropically into a rod. Branched structures could result either from the merger of independently nucleated rods or through growth in multiple directions from a single nucleus. When the simple or branched nanocrystal grows to a sufficient size it detaches from the Au surface. This is expected to occur when the total internal crystal strain energy, due to lattice mismatch between Au and PbSe, becomes sufficiently large, as the length of the rod increases. For example, in a careful electron microscopy study of Ag nanoparticles on Pt surfaces by Ashkenazy et al., it has been shown that small particles below a critical size align epitaxially with the substrate, but above this critical size an array of grain boundary dislocations are created.[20] A similar mechanism would lead to the cleaving of PbSe nanocrystals from the Au surface, ultimately breaking the ternary heterostuctures into a mixture of the binary seed particles with freestanding simple and branched PbSe rods. In support of this mechanism, Figure 1 shows typical TEM images of the PbSe rods in the early stages of growth still attached to the Au–Fe_3O_4 nanoparticles. At a later stage of reaction, provided that sufficient precursors are present, all PbSe rods and Au–Fe_3O_4 hybrid nanoparticles are separated.

The appreciable population of L-, T-, and cross-shaped nanocrystals can be explained by different nucleation events on the Au surface. The branching mechanism may be similar to the geminate nanowire nucleation mechanism described by Kuno and co-workers.[10,11] Nucleation of PbSe on the Au surface can lead to growth perpendicular to or tangential to the seed particle, as illustrated in Figure 1, structures **2a** and **2b**. Multiple rods can also grow out of one seed particle, as seen from structures **3a** and **4a** in Figure 1. All of these configurations can lead to formation of free rods after cleavage from the seed particle. However, if two or three rods nucleate on the particle surface simultaneously, they may be able to merge into a single L- or T-shaped structure prior to cleavage from the seed. These structures can also be interpreted as arising from simultaneous rod growth both perpendicular and tangential to the seed particle. This general picture of the growth process explains the formation of rods and L- and T-shaped particles, but does not fully explain the formation of cross-shaped particles. We do not clearly observe any cross-shaped

particles attached to Au seeds. However, their presence cannot be ruled out, since when attached to a seed particle, they may not orient in a way that makes all four arms visible in TEM. Some structures, like structure **5** of Figure 1, look as if they may have four branches while still attached to the seed particle. It is also possible that one or more new arms grow from the surface that cleaves from the seed particle, after it has cleaved. The plausibility of this mechanism is supported by the fact that the free rods appear to continue growing in the axial direction after cleaving from the seed particles, as shown in Figure 3 for rods extracted after different growth times. This is also consistent with the observation that predominantly branched particles (T- and cross-shaped), rather than simple rods, are formed when the precursor-to-seed particle ratio is increased (by reducing the seed particle concentration). In this case, the higher precursor-to-seed ratio resulted in more cases of multiple nucleation on a single seed particle. A higher precursor concentration thus remains at the time when the nanocrystals reach a critical size and cleave from the seed particles. This might enable rapid growth of one or more additional branches on the reactive face generated by the cleavage of the rod from the seed particle. Conversely, when the seed particle concentration is doubled, the precursors are depleted before the nanocrystals reach a critical size at which they cleave from the seed particle, and ternary hybrid particles are observed.

As shown in Figure 1, structures **2a** and **2b**, a single PbSe rod can form on Au–Fe_3O_4 in either of two configurations: tangential or perpendicular to the seed particle surface. In the free PbSe rods, we observe slight variations in morphology that might be attributed to these different growth modes. Many PbSe rods, like the ones shown in Figure 4a and c, have one pointed end. These may be rods that grow perpendicular to the seed particle surface, with the pointed end representing the point of attachment to the seed particle. A smaller fraction of rods have a thin or defective region in their center that might represent the point of attachment for a rod grown tangential to the seed particle surface. Examples are shown in Figure S3 in the Supporting Information.

The choice of Au–Fe_3O_4 binary particles over pure Au seed particles provides essential advantages in the growth of PbSe nanorods. In the absence of any seed particles, roughly spherical PbSe nanocrystals form under the synthesis conditions used here (see Fig. S4 in the Supporting Information). While Au alone can catalyze the anisotropic growth of PbSe nanocrystals, only a mixture of Au–PbSe core/shell and spherical PbSe nanoparticles is formed under the conditions used in the present study (see Fig. S5 in the Supporting Information). Using pure Au nanoparticles as seeds, PbSe nanorods can only form at seed particle-to-precursor ratios roughly a factor of 50 lower than those used here.[15] This suggests that the role of Fe_3O_4 in the binary seeds is to block a large fraction of the Au surface nucleation sites, so that only anisotropic growth of PbSe can occur, and core/shell structures cannot form. This provides a much more robust and controllable route to PbSe rods. It also allows production of much smaller diameter rods. In the present work, rods with mean diameters of 2.5 and 3.0 nm and aspect ratios of four and six, respectively, were obtained, as shown in Figure 3b and c. In contrast, the smallest particle diameters obtained in a separate study[15] of PbSe rod growth seeded with pure Au nanoparticles was ca. 6 nm. The use of binary seeds also leads to much higher conversion of precursors to PbSe nanocrystals. For pure metal seeding, the rod formation occurs at low reactant conversion, and the total yield is just a few percent of the theoretical yield that would be obtained if all precursors were converted to rods.[15] When using binary seeds the yields are substantially higher (by about a factor of five, although precise yield measurements are difficult in both cases due to particle losses during washing, etc.). There seems to be a corresponding difference in growth mechanism between the pure metal seeds versus the binary particles, since branching increased with increasing seed concentration for pure metal seeds,[15] but decreased with increasing seed concentration for the binary seeds. We believe that this difference is associated with the fact that with the pure metal seeds, growth occurs at low reactant conversion (nearly constant precursor concentration), while with the binary seeds, growth can be allowed to continue until the limiting precursor is substantially consumed. Thus, for the binary seeds, decreasing the seed concentration leads to greater precursor consumption per seed, through the formation of more rods per seed and eventual fusion of these into multibranched structures. The use of binary nanoparticle seeds also allows the capture and direct observation of rods that are still attached to the seed particles, as shown in Figures 1 and 2, which was not possible for pure metal seeding. This may allow clearer elucidation of the nucleation and growth mechanisms than is possible in the case of pure Au nanoparticles where growth and cleavage from the seed particles are much more rapid. Finally, in the case of ternary particles where the PbSe rod is still attached to the binary seed, the Fe_3O_4 component provides a magnetic 'handle' that allows self-assembly of these particles to be guided by the application of a magnetic field.

In addition to allowing preparation of ternary heterostructures combining plasmonic, magnetic, and semiconducting properties in a single multicomponent nanocrystalline particle, seeding with Au–Fe_3O_4 binary hybrid nanoparticles has enabled the growth of PbSe nanorods and branched nanorods with controlled lengths and diameters. By changing the ratio of PbSe precursors to Au–Fe_3O_4 seed particles, PbSe nanocrystals with different morphologies (dots, simple rods, and branched rods) have been obtained. Au acts as a preferred seeding point on a binary structure, and leads to rod growth on the seed particle under conditions where core/shell structures would form on pure Au nanoparticles of the same size. Seeding with binary particles has significant advantages over pure metal seeding, even when single-component anisotropic PbSe nanocrystals are the desired product.

ADVANCED MATERIALS

Experimental

Materials: Hydrogen tetrachloroaurate(III) trihydrate ($HAuCl_4 \cdot 3H_2O$), dodecylamine (98 %), sodium borohydride (powder, 98 %), tetraoctylammonium bromide (98 %), iron(III) acetylacetonate, iron pentacarbonyl, 1-octadecene (90 %), octyl ether (99 %), phenyl ether (99 %), 1,2-hexadecanediol (90 %), lead oxide (99.999 %), selenium (powder), TOP (90 %), oleic acid (90 %), and oleylamine (70 %) were purchased from Aldrich. All chemicals were used as received.

Synthesis of Au Nanoparticles: The Au nanoparticles were synthesized using the Brust two-phase method [21]. By changing the surfactant-to-$HAuCl_4$ ratio, the average size of the Au nanoparticles could be tuned from less than 2 nm up to 20 nm. These particles were purified and used as seeds for further synthesis of Au–Fe_3O_4 peanut hybrid nanoparticles. In subsequent preparations described below, ca. 3 nm Au nanoparticles were used.

Synthesis of Au–Fe_3O_4 Peanutlike Binary Hybrid Nanoparticles: Au–Fe_3O_4 peanut hybrid nanoparticles were synthesized by mixing premade ca. 3 nm Au nanoparticles with $Fe(CO)_5$ in 1-octadecene in the presence of oleic acid and oleylamine, then heating the mixture to reflux (ca. 300 °C) followed by room-temperature oxidation under air as described by Yu et al. [22]. The product, Au–Fe_3O_4 particles, were redispersed in organic solvents such as hexane or toluene.

Synthesis of Simple and Branched PbSe Nanorods: PbSe nanorods were synthesized by reacting the Pb and Se precursors in the presence of Au–Fe_3O_4 peanut hybrid nanoparticles. In a typical synthesis, 0.5 mmol PbO, 2.5 mmol oleic acid, and 10 mL phenyl ether were loaded into a 100 mL three-necked flask set in a heating mantle. Under argon gas flow, the mixture was heated to 120 °C until the Pb-oleate complex was formed (as indicated by the mixture becoming colorless and transparent). Au–Fe_3O_4 peanut-shaped hybrid nanoparticles in hexane (containing ca. 0.0125 mmol Au atoms) were added, and the hexane was then evaporated and removed through a needle outlet. Then 10 mL of 0.1 M selenium in TOP (Se–TOP) was rapidly injected into the reaction mixture at 145 °C. Upon this rapid injection, the temperature dropped to ca. 125 °C, then slowly increased to ca. 135 °C after ca. 10 min. Aliquots were withdrawn from the reaction mixture at various times and quenched with hexane. The samples were washed with acetone under air followed by centrifugation, then redispersed in hexane.

Experiments were also performed with smaller solvent volumes (5 mL phenyl ether instead of 10 mL, and 1 mL of 1 M Se–TOP instead of 10 mL of 0.1 M Se–TOP) and injection of the Se–TOP at 155 °C. In this case, there was no substantial temperature drop upon Se–TOP addition. The reaction took place near 155 °C and was much more rapid.

The amount of Au–Fe_3O_4 seed nanoparticles used in the experiments described above was varied as a means of controlling the ultimate extent of growth via the amount of precursor available to each seed particle. Thus, experiments were also performed following the above procedures, but either doubling or halving the amount of binary hybrid seed nanoparticles used. This yielded ternary heterostructures (at higher seed particle concentration) or branched PbSe nanocrystals (at lower seed particle concentration).

Characterization: TEM images were obtained using a JEOL model JEM-100CX microscope at an acceleration voltage of 80 kV. The specimens were prepared by dropping the nanoparticle dispersion onto an amorphous carbon-coated 300 mesh copper grid and allowing the solvent to evaporate. Electron diffraction and HRTEM images were obtained using a JEOL model 4000EX microscope at an acceleration voltage of 400 kV. UV-VIS-IR absorption was measured using a Shimadzu model 3101 UV-vis-NIR scanning spectrophotometer. Dispersions in tetrachloroethylene were measured against pure tetrachloroethylene as a reference.

Received: March30, 2006
Final version: April 25, 2006

[1] J. F. Wang, M. S. Gudisken, X. F. Duan, Y. Cui, C. M. Lieber, *Science* **2001**, *293*, 1455.
[2] W. U. Huynh, J. J. A. Dittmer, A. P. Alivisatos, *Science* **2002**, *295*, 2425.
[3] X. G. Peng, L. Manna, W. D. Yang, J. Wickham, E. Scher, A. Kadavanich, A. P. Alivisatos, *Nature* **2000**, *404*, 59.
[4] Z. A. Peng, X. G. Peng, *J. Am. Chem. Soc.* **2002**, *124*, 3343.
[5] T. J. Trentler, K. M. Hickman, S. C. Goel, A. M. Viano, P. C. Gibbons, W. E. Buhro, *Science* **1995**, *270*, 1791.
[6] T. J. Trentler, S. C. Goel, K. M. Hickman, A. M. Viano, M. Y. Chiang, A. M. Beatty, P. C. Gibbons, W. E. Buhro, *J. Am. Chem. Soc.* **1997**, *119*, 2172.
[7] H. Yu, J. B. Li, R. A. Loomis, L. W. Wang, W. E. Buhro, *Nat. Mater.* **2003**, *2*, 517.
[8] H. Yu, W. E. Buhro, *Adv. Mater.* **2003**, *15*, 416.
[9] H. Yu, J. B. Li, R. A. Loomis, P. C. Gibbons, L. W. Wang, W. E. Buhro, *J. Am. Chem. Soc.* **2003**, *125*, 16 168.
[10] J. W. Grebinski, K. L. Hull, J. Zhang, T. H. Kosel, M. Kuno, *Chem. Mater.* **2004**, *16*, 5260.
[11] K. L. Hull, J. W. Grebinski, T. H. Kosel, M. Kuno, *Chem. Mater.* **2005**, *17*, 4416.
[12] J. D. Holmes, K. P. Johnston, R. C. Doty, B. A. Korgel, *Science* **2000**, *287*, 1471.
[13] T. Hanrath, B. A. Korgel, *J. Am. Chem. Soc.* **2002**, *124*, 1424.
[14] K. S. Cho, D. V. Talapin, W. Gaschler, C. B. Murray, *J. Am. Chem. Soc.* **2005**, *127*, 7140.
[15] K.-T. Yong, Y. Sahoo, K. R. Choudhury, M. T. Swihart, J. R. Minter, P. N. Prasad, *Nano Lett.* **2006**, *6*, 709.
[16] S. Kan, T. Mokari, E. Rothenberg, U. Banin, *Nat. Mater.* **2003**, *2*, 155.
[17] W. Shi, H. Zeng, Y. Sahoo, T. Y. Ohulchanskyy, Y. Ding, Z. L. Wang, M. T. Swihart, P. N. Prasad, *Nano Lett.* **2006**, *6*, 875.
[18] K. Dick, T. Dhanasekaran, Z. Y. Zhang, D. Meisel, *J. Am. Chem. Soc.* **2002**, *124*, 2312.
[19] E. A. Brandes, G. B. Brook, Smithells Metals Reference Book, 7th ed., Butterworth-Heinemann, Boston **1998**.
[20] Y. Ashkenazy, R. S. Averback, K. Albe, *Phys. Rev. B* **2001**, *64*, 205 409.
[21] M. Brust, M. Walker, D. Bethell, D. J. Schiffrin, R. Whyman, *J. Chem. Soc. Chem. Commun.* **1994**, 801.
[22] H. Yu, M. Chen, P. M. Rice, S. X. Wang, R. L. White, S. H. Sun, *Nano Lett.* **2005**, *5*, 379.

